

Understanding and mapping the assembly of a family of trimeric polyoxometalates: transition metal mediated Wells-Dawson (M_{18})-trimers†

Thomas Boyd, Scott G. Mitchell, Haralampos N. Miras, De-Liang Long and Leroy Cronin*

Received 9th February 2010, Accepted 19th April 2010

First published as an Advance Article on the web 9th June 2010

DOI: 10.1039/c002633f

Four iso-structural triple Wells-Dawson-type phosphotungstate compounds incorporating six transition metal ion linkers are presented of the form $[(M_2P_2W_{16}O_{60})_3]^{24-/30-}$, **1–4**, where $M = Co, Mn, Fe, Ni$ respectively and compounds **3** and **4** are revealed for the first time uniting a family of isostructural clusters. Further, a comparative study of the solid-state arrangements of polyoxoanions **1–4** is presented as well as an in-depth discussion of the synthetic conditions which give rise to the formation of the clusters. Each cluster subunit displays an unprecedented diequatorial substitution pattern facilitating the combination of three such units into a trimer, creating central cavities in the range 6.61–6.82 Å. The solid state arrangements of polyoxoanions **1**, **3** and **4** are similar, but as a result of the relevant synthetic approaches, they differ greatly from that of **2**. Electrochemical analysis of the new structures is detailed revealing that polyoxoanion **4** shows potential as an electrocatalyst in the reduction of nitrites.

Introduction

The general principles for synthesizing polyoxometalates (POMs), discrete clusters of early transition metal-oxo units, are synthetically well-defined in terms of the practical synthesis, but still mysterious regarding the mechanism of self assembly.¹ This mystery is eased slightly in tungstate-based POM chemistry since certain structural motifs form a well known building block library such as the Wells-Dawson polytungstate anion $[X_2W_{18}O_{62}]^{6-}$ (where X is a tetrahedral template such as P^v or As^v), first structurally investigated in 1953.² Lacunary POMs are structural derivatives of saturated, plenary clusters, containing gaps or voids. These structural defects convey an enhanced surface reactivity, making lacuna highly versatile and applicable as secondary building units (SBUs) in the construction of POM assemblies.³ Further, several lacunary derivatives of the Wells-Dawson octadecatungstodiphosphate polyanion (abbreviated as $\{P_2W_{18}\}$) have been identified, with the degree of degradation dependant on both pH, and the type of cations present.⁴

Structures ranging from monolacunary ($M_{18} - M_1$ i.e. M_{17}) to hexalacunary ($M_{18} - M_6$ i.e. M_{12}) have been isolated and characterised, whilst site-specific vacancies can also be accessed via molybdenum substitution.⁵ The hexavacant Wells-Dawson cluster $\alpha-[P_2W_{12}O_{48}]^{14-}$ (abbreviated as $\{P_2W_{12}\}$) has been utilised in the assembly of larger, dimeric,⁶ trimeric⁷ and tetrameric⁶ aggregates arranged as open or crown-type structures. If further architectures based on simple $\{P_2W_{12}\}$ aggregates are to be realised, the propensity for a seemingly limited selection of inter-subunit bonding angles must be overcome.

Owing to their strongly anionic nature, lacunary POMs can effectively bind transition metals (TMs) with an outstanding range of nuclearities and diverse structural topologies currently realised.⁸ Incorporation of TM centres in lacunary POM sites is a key strategy for the development of novel, functional POM assemblies. A great number of $\{P_2W_{12}\}$ -based transition metal-substituted polyoxometalates (TMSPs) have been reported recently, such as the multi-iron complexes prepared by Gouzerh and co-workers,⁹ the heart-shaped, cobalt-linked dimer reported by Wang and co-workers¹⁰ and the plethora of tetrameric $\{P_8W_{48}\}$ assemblies encapsulating central TM ions.¹¹ Such TMSPs are of great interest, particularly due to their potential as single-molecule magnets (SMMs) or as catalysts.^{12–13} The establishment of structurally well-defined classes, or families, of compounds is necessary to exhibit control in these applications, giving the material tuneable properties. Despite well-adapted design principles, allowing some control to prepare such iso-structural materials, pre-defined structural control has been notoriously difficult in polyoxometalate chemistry. In particular, the site-selective substitution of tungsten addenda atoms for TMs in the Wells-Dawson framework is frequently unreliable.¹⁴ Commonly, substitution in the equatorial belt region is accompanied by substitution in the polar cap, although exclusive belt substitution in sandwich complexes has been demonstrated.¹⁵ TM atoms have also shown a tendency to migrate from cap to belt position during the recrystallization of monosubstituted TM-Wells-Dawson derivatives.¹⁶

The most widely utilised synthetic strategy to obtain highly-substituted TMSPs based on $\{P_2W_{12}\}$, has involved mixing solutions of the polyvacant cluster with simple transition metal salts at low pH.¹⁷ In an attempt to trap transition metal ions in vacant lacunary sites of $\{P_2W_{12}\}$, we adopted a new approach adapted from the synthetic route from $\{P_2W_{18}\}$ to $\{P_2W_{12}\}$.¹⁸ The result was our recently reported trimeric Wells-Dawson assembly incorporating six cobalt centres.¹⁹

Polyoxoanion $[(Co_2P_2W_{16}O_{60})_3]^{24-}$ (**1a**) consists of three α -isomer Wells-Dawson units, each containing two Co^{3+} ions, connected through equatorial $\{Co-O-W\}_2$ bridges (Fig. 1). The distinctive

WestCHEM, Department of Chemistry, University of Glasgow, Joseph Black Building, University Avenue, Glasgow, UK G12 8QQ. E-mail: L.Cronin@chem.gla.ac.uk; Web: www.croninlab.com; Fax: +44 (0) 141 330 4888; Tel: +44 (0) 141 330 6650

† Electronic supplementary information (ESI) available: figures S1–S6 and table S1. CCDC reference numbers 765772 and 765773. For ESI and crystallographic data in CIF or other electronic format see DOI: 10.1039/c002633f

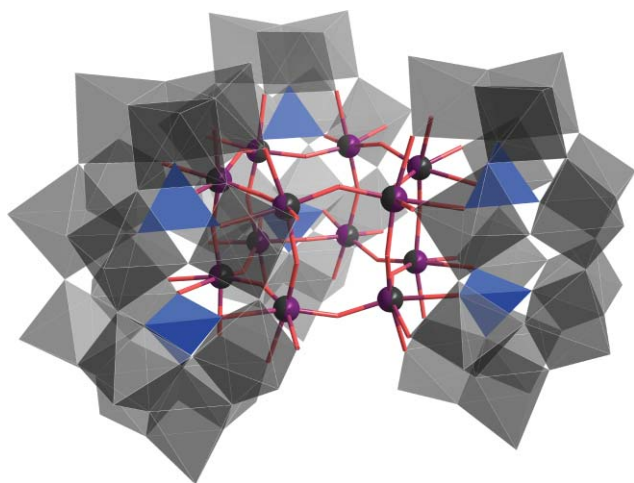


Fig. 1 The trimeric Wells-Dawson polyanion structure of compounds **1–4**, of general formula $[(M_2P_2W_{16}O_{60})_3]^{24-30-}$; here illustrated by polyanion $[(Co_2P_2W_{16}O_{60})_3]^{24-}$ (**1a**), a trimeric assembly of three Co^{3+} di-substituted Wells-Dawson cluster species. The central core is highlighted with 12 mixed-occupancy Co^{3+}/W^{6+} sites. Each Wells-Dawson subunit is linked through $\{Co-O-W\}_2$ connectivities to give a distinct triangular topology. Dark grey/purple spheres: W/Co mixed-occupancy sites; light red sticks: oxygen; light grey octahedra: WO_6 ; blue tetrahedra: PO_4 .

triangular topology evident in this structure was replicated in concurrent work, published by Wang and co-workers, of an analogous triple-Wells-Dawson polyanion containing two Mn^{3+} metal atom linkers per subunit.²⁰ $[(Mn_2P_2W_{16}O_{60})_3]^{24-}$ (**2a**) has an identical structural arrangement to **1**, comprising three Wells-Dawson units encompassing a hexamanganese-substituted, twelve-membered, double-ring core. Here we report an important expansion of this family with two further TMSPs of the same class, $[(H_2Fe_2P_2W_{16}O_{60})_3]^{24-}$ (**3a**) and $[(Ni_2P_2W_{16}O_{60})_3]^{30-}$ (**4a**), incorporating Fe^{2+} and Ni^{2+} respectively. Further, the elucidation of these structures allows us to compare and contrast the synthetic methodology used in the preparation of these novel clusters, together with a study of both their discrete structures, solid state arrangements and their physical properties with the existing compounds. This comparison provides a unique structural and mechanistic insight to these clusters and leads to some general conclusions with broad implications and perspectives for the designed assembly of POM-based nanoscale aggregates using lacunary precursors.

Experimental

Starting materials, methods and measurements

Isomerically pure Wells-Dawson-type cluster, $K_6[\alpha-P_2W_{18}O_{62}]\cdot 14H_2O$ was obtained by the high-yielding, two-step method reported in the literature.²¹ All other reagents were used as purchased. For single-crystal X-ray diffraction, suitable single crystals were selected and mounted onto the end of a thin glass fibre using Fomblin oil. X-ray diffraction intensity data for compounds **3** and **4** were collected using an Oxford Diffraction Gemini Ultra with an ATLAS charge-coupled device (CCD) detector [$\lambda(Mo-K\alpha) = 0.71073 \text{ \AA}$; $\lambda(Cu-K\alpha) = 1.54184 \text{ \AA}$] at 150(2) K. Data reduction was performed using the CrysAlis software package and structure solution, and

refinement was carried out using SHELXS-97²² and SHELXL-97²³ using WinGX.²⁴ Corrections for incident and diffracted beam absorption effects were applied using analytical numeric absorption correction using a multifaceted crystal model.²⁵ Infrared spectra were measured using samples dispersed in a KBr disk on a Jasco FTIR-410 spectrometer. Wavenumbers are given in cm^{-1} and peaks denoted as strong (s), weak (w) or broad (b). UV-Vis spectra were recorded using a Shimadzu UV-3101PC spectrophotometer in transmission mode with quartz cuvettes of optical path length 1.0 cm. FAAS measurements were performed on a Perkin-Elmer 1100B Atomic Absorption Spectrophotometer, whilst a Corning Flame Photometer 410 was used to determine Na^+ and K^+ content of the materials. Carbon, hydrogen and nitrogen content were determined with an EA 1110 CHNS, CE440 Elemental analyser. Thermogravimetric Analysis (TGA) was performed on a TA Q500 instrument under an atmosphere of nitrogen, with initial heating at a rate of 2.00 °C per minute from room temperature to 150 °C followed by a rate of 5.00 °C for the range 150 °C to 1000 °C. Voltammograms were obtained using a Model Versastat 4 electro analysis system by Princeton Applied Research. The standard three-electrode arrangement was employed with a Pt mesh auxiliary electrode, 1.5 mm glassy carbon working electrode, and Ag/AgCl/KCl reference electrode at room temperature ($19 \pm 1 \text{ }^\circ\text{C}$). All potentials are quoted relative to the Ag/AgCl/KCl reference electrode. The glassy carbon working electrodes (diameter 1.5 mm) were polished with alumina (3 μm) on polishing pads, rinsed with distilled water and sonicated in H_2O and then acetone solution before each experiment. The cell was purged with Ar for at least 10 min before each experiment.

Synthesis of compounds **3** and **4**

Preparation of $Na_{22}K_2[(H_2Fe_2P_2W_{16}O_{60})_3]\cdot 67H_2O$ (3**).** $K_6[\alpha-P_2W_{18}O_{62}]\cdot 14H_2O$ (10.38 g, 2.14 mmol) was dissolved in 37.5 mL H_2O whilst, in a separate flask, tris(hydroxymethyl)aminomethane (TRIS base) (6.05 g, 0.05 mmol) was dissolved in 25 mL H_2O . When all the solid material had been completely dissolved and both solutions were clear, the TRIS base solution (pH 11.10) was poured directly into the POM solution (pH 3.93) and allowed to stir for exactly 30 min, to give a clear, colourless solution of pH 8.40. Meanwhile, $FeCl_2\cdot 4H_2O$ (10.34 g, 0.05 mmol) was added to 50 mL of water with vigorous stirring, giving a thick brown sludge-like precipitate. After a short period of stirring, this was added to the POM-TRIS solution, producing a sandy brown precipitate. The reaction mixture was allowed to stir for a further 15 min before centrifugation to isolate the precipitate, which was subsequently dried overnight *in vacuo*. Recrystallization of the crude material (11.74 g) was achieved by dissolving a 2 g sample in 200 ml of a hot aqueous 1M NaCl solution and adjusting the pH from a natural pH of 3.58, to exactly 7.00 with a few drops of 1M NaOH. Filtration was required to remove a small amount of undissolved crude material, resulting in a clear yellow solution, which was again filtered after one day to remove a small amount of fine brown precipitate. Well-formed sandy brown rectangular crystals appeared in solution after 7 days, and were collected by Büchner filtration after 10–14 days. Yield (from 2 g of crude product): 0.15 g, 0.011 mmol (9% based on W). Characteristic IR-bands: 3389(b), 1619(s), 1078(s), 1009(w), 952(s), 908(s), 768(s),

663(w), 512(w). UV-bands, nm (ϵ): 740 (4.58). Elemental analysis for the hydrated material, $\text{H}_{140}\text{Fe}_6\text{K}_2\text{Na}_{22}\text{O}_{247}\text{P}_6\text{W}_{48}$, $\text{MW} = 14022.82 \text{ g mol}^{-1}$. Calculated values (actual values in brackets): Fe: 2.39 (2.58), W: 62.95 (59.90),²⁶ K: 0.56 (0.50), Na: 3.61 (3.58)%. TGA measurement showed water loss from 25 to 300 °C, calculated (found): 8.60 (8.64%).

Preparation of $\text{Na}_{28}\text{K}_2[(\text{Ni}_2\text{P}_2\text{W}_{16}\text{O}_{60})_3]\cdot 91\text{H}_2\text{O}$ (4). The POM-TRIS solution was prepared in exactly the same way as for compound 3. Concurrently, $\text{NiCl}_2\cdot 6\text{H}_2\text{O}$ (12.36 g, 0.052 mmol) was dissolved in 25 mL of water to give a clear, apple-green solution. This was added to the POM-TRIS solution to instantly produce a thick slurry-like pale blue/green precipitate, and allowed to stir for 15 min. The mixture was separated by Büchner filtration and the blue/green precipitate was washed with ethanol, and subsequently dried overnight *in vacuo*. The dry, crude product (9.30 g) was recrystallized by dissolving a 2 g sample in 200 mL of a hot aqueous 1M NaCl solution, resulting in a clear light green coloured solution at pH 7.34. Rectangular, pale green crystals of 4 appeared in solution after 48 h and were collected by Büchner filtration after 3 days. Yield (from 2 g of crude product): 0.433 g, 0.030 mmol (20% based on W). Characteristic IR-bands: 3418(b), 1623(s), 1086(s), 1063(s), 1006(w), 945(s), 902(s), 798(s), 724(s), 488(w). UV-bands, nm (ϵ): 739 (55.14). Elemental analysis for the hydrated material, $\text{H}_{182}\text{K}_2\text{Na}_{28}\text{Ni}_6\text{O}_{271}\text{P}_6\text{W}_{48}$, $\text{MW} = 14604.26 \text{ g mol}^{-1}$. Calculated values (actual values in brackets): Ni: 2.38 (2.47), W: 60.47 (60.27), K: 0.53 (0.55), Na: 4.41 (3.86)%. TGA measurement showed water loss from 25 to 300 °C, calculated (found): 11.35 (11.27%).

Discussion

Synthesis

The general synthetic method employed in the preparation of compounds 3 and 4 was the same as used previously for compound 1, which is interesting since it may allow us to develop a general approach to both design and isolate these new TMSPs. This is because the mechanism of formation of compounds 1, 3 and 4 appears to proceed *via* the tris(hydroxymethyl)aminomethane (TRIS base)-mediated removal of 6 addenda tungsten atoms from the primitive Wells-Dawson unit, giving the $\{\text{P}_2\text{W}_{12}\}$ lacuna, which is not isolated. Functionalisation of $\{\text{P}_2\text{W}_{12}\}$ *in situ* in this manner therefore is a robust approach to TMSPs based on this building block. The addition of an excess amount of transition metal salt to the reaction mixture produces an amorphous precipitate, which, when isolated and dried, causes the solution pH (unbuffered) to become 3.58 for 3 and 7.34 for 4. In this instance, the transition metal salt has two primary functions; first, the insertion of two transition metal centres into the belt region of each $\{\text{P}_2\text{W}_{12}\}$ building block, and second, promoting re-inclusion of four $\{\text{WO}_6\}$ octahedra into each sub-unit to re-establish the Wells-Dawson-type structure. The availability in solution of $\{\text{WO}_6\}$ fragments for re-insertion is supplemented by the one-pot, disassembly-reassembly process occurring here. The markedly lower pH of the crude material of compound 3 in solution is thought to be a result of hydrolysis of water ligands coordinated to the transition metal salt. Analysis of the carbon, hydrogen and nitrogen content of compounds 3 and 4 suggest that there are no TRIS-based

cations in the final products. A summative diagram of the reaction pathways in the formation of 3 and 4 is given (Fig. 2).

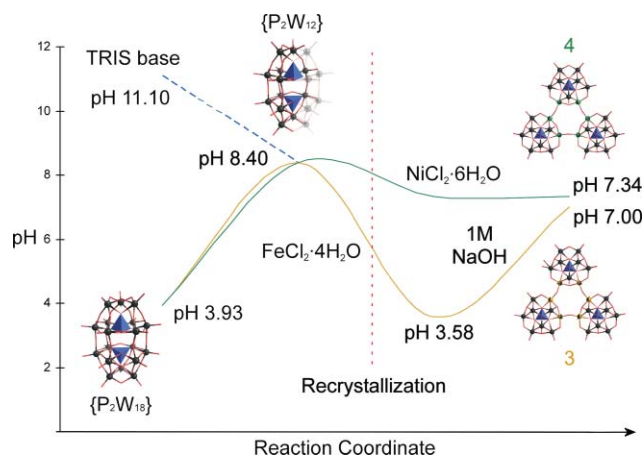


Fig. 2 Charting the pH change with reaction progression for compounds 3 and 4. For both compounds, a TRIS base solution at pH 11.10 is added to a solution of $\{\text{P}_2\text{W}_{18}\}$ at pH 3.93. This raises the cluster solution to pH 8.40, forming $\{\text{P}_2\text{W}_{12}\}$ *in situ*. Addition of the transition metal salt to this solution causes instant precipitation of the crude product. In solution, the crude product of only compound 3 is acidic. Raising the pH of the parent solution of 3 from 3.58 to 7.00 is required to obtain the product in good yield, whilst compound 4 is formed without modification, at pH 7.34.

Wang and co-workers employed a different synthetic method for the preparation of compound 2, whereby the pre-formed lacunary cluster $\alpha\text{-}[\text{P}_2\text{W}_{12}\text{O}_{48}]^{14-}$ was introduced to a mixed transition metal/lanthanide/acetate solution system. Effectively, this method requires an additional step; $\{\text{P}_2\text{W}_{12}\}$ is formed and isolated by amine and K_2CO_3 degradation of $\{\text{P}_2\text{W}_{18}\}$ before being reacted with the other components. The more complex solution system provides redox active Ce^{4+} and Mn^{2+} ions which combine in acidic conditions to form a bipyramid-like cation template. Notably, we have been unsuccessful in recrystallizing the Mn-trimer using our synthetic procedure, instead forming only amorphous precipitate and Na salts despite an extensive number of experiments due to the very fast precipitation of the products under these conditions.

Structural analysis

This work therefore shows that compounds 3 and 4 result from the TRIS base-mediated decomposition of $\{\text{P}_2\text{W}_{18}\}$ before re-assembly, incorporating two transition metal centres per unit. The result is an effective substitution of two addenda tungsten atoms of the plenary Wells-Dawson cluster anion with first-row transition metal atoms M ($\text{M} = \text{Fe}^{2+}, \text{Ni}^{2+}$). Of the six sites vacated during TRIS base decomposition, the first row transition metal is distributed evenly across the four equatorial positions, with occupancy at each of these sites determined to be 50% W and 50% M. The equatorial location of the inserted transition metal is consistent with previous reports of $\{\text{P}_2\text{W}_{12}\}$ reassembly, although the incorporation of two metal centres is unusual.

The solid state arrangements of polyanions 1–4 were investigated by analysis of the crystal packing of each structure (Fig. 3, Table 1). In each cluster assembly, the double ring of the TM-substituted core is oriented uniformly throughout the structure, with only the relative location of each unit in space

Table 1 Structural data summary for compounds **1–4** (N.B. Compounds **1–2**,^{19,20} previously published, are included here for comparison)

| | 1 ¹⁹ | 2 ²⁰ | 3 | 4 |
|--|--|---|--|--|
| Empirical formula | H ₁₄₆ Co ₆ K ₃ Na ₂₁ O ₂₅₃ P ₆ W ₄₈ | C ₂₄ H ₅₄ Ce ₆ Mn ₁₀ Na ₂₀ O ₂₅₅ P ₆ W ₄₈ | H ₁₄₀ Fe ₆ K ₃ Na ₂₂ O ₂₄₇ P ₆ W ₄₈ | H ₁₈₂ K ₂ Na ₂₈ Ni ₆ O ₂₇₁ P ₆ W ₄₈ |
| <i>F</i> _w (g mol ⁻¹) | 14159.46 | 15283.21 | 14022.82 | 14604.26 |
| Crystal system | Triclinic | Hexagonal | Triclinic | Triclinic |
| Space group | <i>P</i> $\bar{1}$ | <i>P</i> 6 ₃ / <i>mcm</i> | <i>P</i> $\bar{1}$ | <i>P</i> $\bar{1}$ |
| <i>a</i> (Å) | 17.2294(2) | 24.959(4) | 17.5835(5) | 17.1003(3) |
| <i>b</i> (Å) | 25.6034(4) | 24.959(4) | 20.6617(3) | 25.5173(4) |
| <i>c</i> (Å) | 28.8610(5) | 26.923(5) | 36.5786(7) | 28.8698(5) |
| α (°) | 79.469(2) | 90.00 | 89.8110(10) | 79.6680(10) |
| β (°) | 87.590(2) | 90.00 | 82.173(2) | 87.7220(10) |
| γ (°) | 83.489(2) | 120.00 | 75.046(2) | 83.4630(10) |
| <i>V</i> (Å ³) | 12433.33(3) | 14525(4) | 12712.5(5) | 12310.2(4) |
| <i>Z</i> | 2 | 2 | 2 | 2 |
| ρ_c (g cm ⁻³) | 3.770 | 3.495 | 3.663 | 3.940 |
| μ (mm ⁻¹) | 22.729 ^a | 20.420 ^a | 22.167 ^a | 43.013 ^b |
| <i>T</i> (K) | 150(2) | 150(2) | 150(2) | 150(2) |
| No. of reflections (measured) | 118924 | 107511 | 136944 | 105266 |
| No. of reflections (unique) | 38601 | 5899 | 46974 | 43489 |
| <i>R</i> _{int} | 0.0912 | 0.1399 | 0.1112 | 0.0612 |
| Residuals: <i>R</i> _{1(obs)} ; <i>R</i> _{w2(all data)} | 0.0630; 0.15430 | 0.0557; 0.0910 | 0.0677; 0.1785 | 0.0645; 0.1983 |

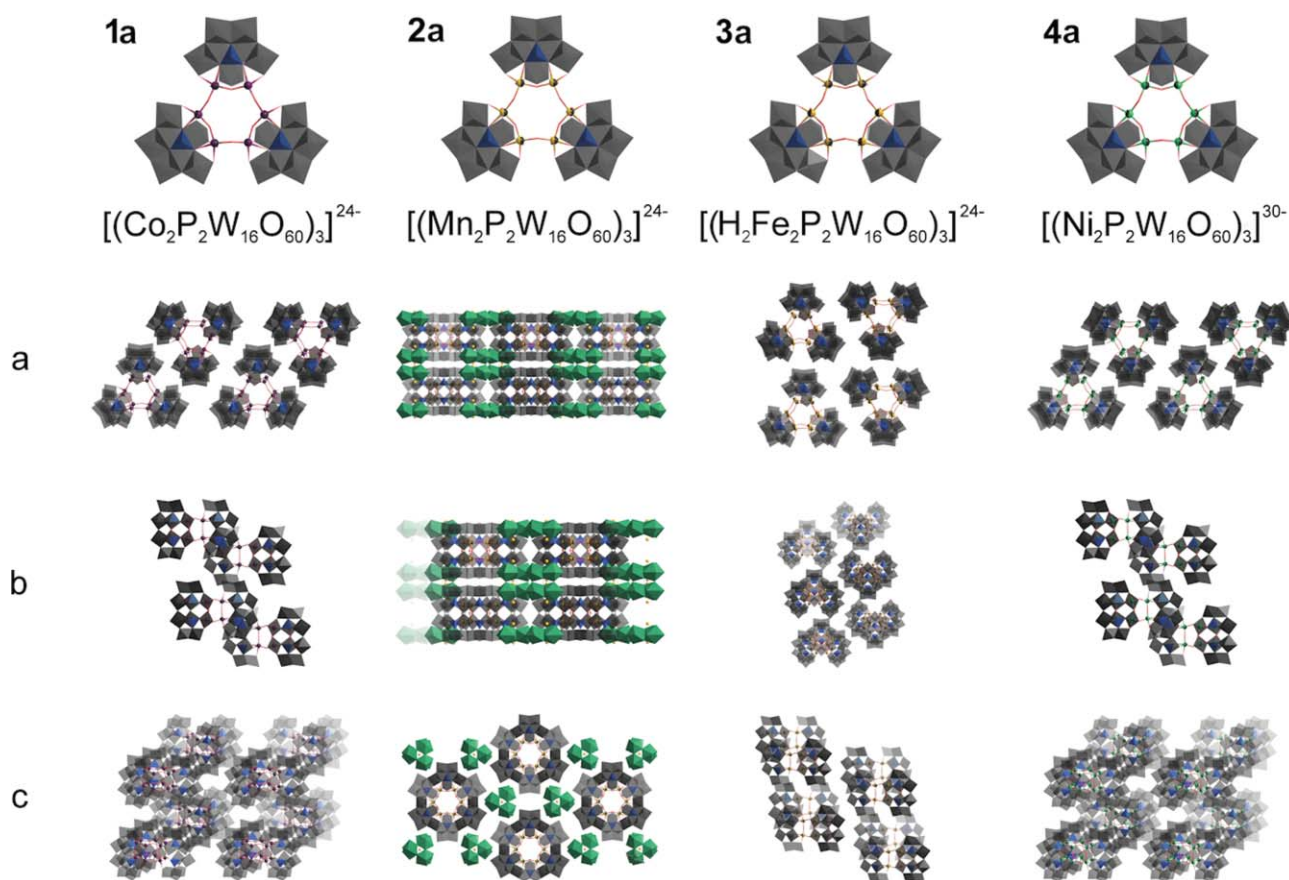
^a Mo-K α ; ^b Cu-K α 

Fig. 3 The crystal packing arrangements of polyanions **1a–4a**, showing each individual trimeric assembly, and their packing along the *a*, *b* and *c* axes respectively. Eight Wells-Dawson trimer units are shown in each picture. Heterometallic Ce⁴⁺/Mn²⁺ clusters are included in the packing of polyanion **2a** to show the templating role of these cationic units in the formation of the Wells-Dawson trimer. All other cations and solvent water molecules are omitted for clarity. All halved spheres are W/TM mixed-occupancy sites where dark grey = W, purple = Co, yellow = Mn, sandy brown = Fe and green = Ni. Otherwise, light red sticks: oxygen; grey octahedra: WO₆; blue tetrahedra: PO₄; green heptahedra: CeO₇; yellow spheres: Mn. (NOTE - polyanions **1a–2a**,^{19,20} previously published are here for comparison).

and the planar rotational position of the trigonal unit varied between the compounds. The trimers can only be oriented one of two ways in the plane, with a difference of 60° between them. A consequence of the inherent threefold symmetry of each trimeric unit, this relationship is analogous to that between isomers of discrete Wells-Dawson clusters, where α and β structures are interconverted by a 60° rotation of the trigonal $\{W_3O_{13}\}$ caps.

Viewing polyanion **1a** along the crystallographic a axis (from above) shows the interpenetration of α and β -oriented trimers in a paired row with minimum spacing of 2.87 Å between the units. From a viewing direction along the b and c axes (side-on), a slightly offset columnar alignment of identically oriented trimers is observed. In compound **2**, the supramolecular packing of the polyanion with cationic Ce^{4+}/Mn^{2+} clusters shows a more pronounced columnar arrangement. Polyanionic cluster units of **2a** are stacked on top of each other in ABAB fashion according to orientation. Layers of identically-oriented trimers can also be observed along the a and b axes. In compound **3**, the packing is related to that of **1** since the Fe^{2+} -substituted structure is similarly tilted, although a more linear alignment of trimers with both the same and opposite orientations can be seen. The supramolecular packing in **4** is almost identical to that of **1**, with a minimum inter-cluster spacing of 2.95 Å.

In compounds **1**, **3** and **4**, K^+ ions act as the ideal template, guiding formation of the trimer from its situation in the central cavity, whereas the formation of compound **2** is independent of a central template, with Na^+ as the sole alkali metal cation surrounding the POM assembly. Heteropolyanion **1a** has the largest central cavity of the four clusters at *ca.* 6.82 Å, contrasting with **3a** at *ca.* 6.61 Å, whilst polyoxoanions **2a** and **4a** have similar central void spacings at *ca.* 6.75 Å and *ca.* 6.72 Å respectively (see Fig. 4 and ESI, Table S1†). The cavity is defined by the pre-formed α - $[M_2P_2W_{16}O_{60}]^{10-}$ SBUs, which are fused through six $\{M-O-W\}$ bridges in two congruent rings of metal centres, to give a trimeric Wells-Dawson-type polyoxoanion. Two protons are associated with each cluster sub-unit in compound **3**, with elongated

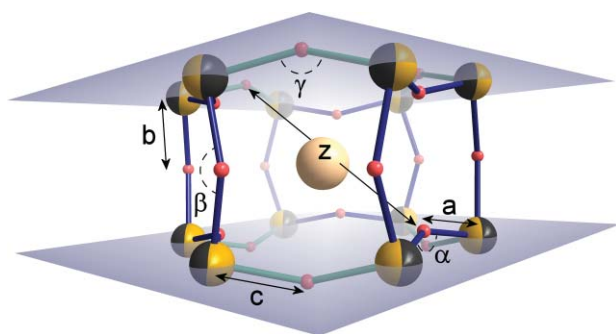


Fig. 4 A close-up of the central core of compounds **1–4**, here illustrated by the Fe^I -substituted polyanion **3a**. Bonds labelled a and b represent intra-subunit bond lengths where a = intra-subunit $W/TM-O_{eq}$ and b = intra-subunit $W/TM-O_{ax}$, whilst c represents inter-subunit $W/TM-O$ bond distances. The related bond angles are labelled α , β and γ . Minimum cavity size, measured between the closest points directly opposite on the two congruent rings, is designated z . All intra-subunit bonds are shown in blue, inter-subunit bonds in green. Dark grey/yellow spheres: W/Fe mixed-occupancy sites; light red spheres: oxygen; tan sphere: potassium. The average values are; a – 1.85; b – 1.86; c – 1.88 Å; α – 149; β – 151; γ – 148°; z – 6.73 Å (see ESI for a full table of values for **1–4**†).

$\{Fe-O-W\}$ bond lengths and less obtuse $\{Fe-O-W\}$ bond angles in relation to the other structures indicative of hydroxy bridging.

Electrochemistry

To further investigate compounds **3** and **4**, and their aqueous solution stability, the redox properties of **3** and **4** were investigated by cyclic voltammetry. To do this, the compounds were dissolved in a buffered aqueous solution and kept at room temperature and the electrochemical behaviour of the solutions was monitored for a 24 h period, during which time no voltammetric characteristics had changed. This characterization provides an initial indication that the compounds are structurally stable under the experimental conditions, as dissolved. Figs. S5 and S6 show the main characteristic peaks associated with W centred redox couples in the region -1.000 to $+1.250$ V of potential values *vs.* $Ag/AgCl$ at a scan rate of 25 and 50 $mV s^{-1}$ respectively. The form of the diagram remained identical regardless of the scanning potential direction, indicating that the phenomena observed in one domain had a negligible influence on those in the other domain.

At the aforementioned scan rate and scanning towards the negative region of potential values, the reduction of W centres for polyoxoanion **3** occurs through four closely-spaced quasi-reversible steps, with the corresponding $E_{1/2}$ peak potentials located respectively at -0.186 , -0.489 , -0.625 and -0.738 V (*vs.* $Ag/AgCl$) while in the positive region of potentials an electrochemically irreversible oxidation for $Fe^{2+} \rightarrow Fe^{3+}$ was observed. As expected, in the case of compound **4**, no oxidation peaks were observed in the positive region indicating that the Ni atoms remained at their initial oxidation state of II. Also, four well-separated W -centred reduction couples were observed, located at $E_{1/2}$ peak potentials of -0.480 , -0.582 , -0.715 and -0.885 V respectively. This study shows the direct effect that the electropositive transition hetero metals have on the W -centred redox couples. In the case of compounds **1**, **3** and **4** the observed redox couples were shown to be shifted towards more negative potentials, reflecting the difficulty in reducing the clusters following the trend $Co^{3+} > Fe^{2+} > Ni^{2+}$. As was expected, the redox couples of the compounds appeared in a similar region of potentials. In comparison with the redox couples which have been observed under similar experimental conditions for the $\{P_2W_{18}\}$ and $\{P_2W_{12}\}$ species a considerable shift for the first two couples towards more negative potentials has been detected. As has been reported previously,²⁷ the existence of a hetero-metal affects considerably the redox potentials, enhancing their oxidizing ability, which could be potentially desirable in catalytic processes.

Electrocatalytic reduction of nitrites

Interest in NO_x has grown considerably ever since its important role in biology, the environment, and industry was unveiled. Generally, it is difficult to directly electro-reduce the nitrite ions, because this process requires a high overpotential. However, the introduction of catalysts, such as POMs, could speed up the electro-reduction process and lower the potential.²⁷ Inspired by the work of Nadjo,^{27–29} and given the activity of our previously reported isostructural cobalt compound (here labelled as compound **1**)¹⁹ towards the reduction of NO_x , we decided to study compounds **3** and **4**.

Upon addition of NaNO₂ in the same medium for both compounds, the cathodic current of the W-centred waves of **3** and **4** is enhanced (see Figs. S3 and S4 respectively in the ESI†), while the corresponding anodic current disappears in both cases. This observation is indicative of electro-catalytic behaviour against nitrites. Comparatively, no reduction of nitrite took place on the GC electrode in the absence of the clusters. Furthermore, using the following equation we could give an extent of the catalytic efficiency of the aforementioned compounds:

$$\text{CAT} = 100 \times [I_p(\text{HPA, NaNO}_2) - I_p(\text{HPA})] / I_p(\text{HPA})$$

where $I_p(\text{HPA})$ is the peak current for the reduction of the heteropolyanion (HPA) in the absence of NaNO₂, and $I_p(\text{HPA, NaNO}_2)$ is the value of the peak current observed in the presence of NaNO₂. The preliminary semi-quantitative studies show that the catalytic efficiency follows the same trend as the reducing difficulty above, $\text{Co}^{3+} > \text{Fe}^{2+} > \text{Ni}^{2+}$. Comparing compounds **1** (from previously published data),¹⁹ **3** and **4**, showed that all compounds give intense electrocatalytic effects and a fully quantitative comparison will be presented later.

Conclusions

Two iso-structural, trimeric Wells-Dawson-type polyoxoanions with the formula $[(\text{H}_x\text{M}_2\text{P}_2\text{W}_{16}\text{O}_{60})_3]^{(30-3x)-}$ where $\text{M} = \text{Fe}$, $x = 2$ (**3**) and $\text{M} = \text{Ni}$, $x = 0$ (**4**) have been synthesized. These two compounds are analogous to the previously published polyanions of the same general formula, where $\text{M} = \text{Co}$ (**1**) and Mn (**2**) respectively. Not only do these new compounds show interesting structural aspects, they expand and unite a family of trimeric clusters, whereby the clusters have an unprecedented diequatorial substitution pattern. Given the similar structure types, we were able to compare and contrast synthetic approaches and conditions used to assemble the clusters, and to map the synthetic route to the assembly of the clusters as a function of reaction coordinate and pH. This clearly shows that for compounds **3** and **4**, when a TRIS base solution is added to a solution of $\{\text{P}_2\text{W}_{18}\}$ at a well defined pH, the reactive $\{\text{P}_2\text{W}_{12}\}$ forms *in situ*. If this is followed by the addition of the transition metal salt, this leads to the formation of the cluster-trimers and the instant precipitation of a crude material, which can be recrystallized to form the presented compounds.

In future work we will try to identify the intermediate species in this disassembly-reassembly process, characterize the crude material that was obtained and isolate further compounds of the same class. We will also look to utilise the reliable *in situ* formation of $\{\text{P}_2\text{W}_{12}\}$ to attempt to insert hetero-metals into other positions on the Wells-Dawson cage and link them in a designed way to produce novel types of molecules, materials, and even utilise $\{\text{P}_2\text{W}_{12}\}$ as an SBU to produce new types of inorganic frameworks.

References

- 1 M. T. Pope, *Heteropoly and Isopoly Oxometalates*, Springer, Berlin, 1983; D.-L. Long, R. Tsunashima and L. Cronin, *Angew. Chem. Int. Ed.*, 2010, 49, 2; L. Cronin, P. Kögerler and A. Müller, *J. Solid. State. Chem.*, 2000, 152, 57.
- 2 B. Dawson, *Acta Crystallogr.*, 1953, 6, 113.
- 3 D.-L. Long, E. Burkholder and L. Cronin, *Chem. Soc. Rev.*, 2007, 36, 105.

- 4 C. Tourné and G. Tourné, *Bull. Soc. Chim. Fr.*, 1969, 4, 1124; R. Contant and J. P. Ciabrini, *J. Chem. Res.*, 1977, (M) 2601; R. Contant and J. P. Ciabrini, *J. Chem. Res.*, 1977, (S) 222; R. G. Finke and M. W. Droegge, *Inorg. Chem.*, 1983, 22, 1006.
- 5 R. Contant and J. P. Ciabrini, *J. Inorg. Nucl. Chem.*, 1981, 43, 1525.
- 6 R. Contant and A. Tézé, *Inorg. Chem.*, 1985, 24, 4610.
- 7 Z.-M. Zhang, S. Yao, Y.-G. Li, Y.-H. Wang, Y.-F. Qi and E.-B. Wang, *Chem. Commun.*, 2008, 1650.
- 8 C. Ritchie, T. Boyd, D.-L. Long, E. Ditzel and L. Cronin, *Dalton Trans.*, 2009, 1587; B. Botar, P. Kögerler and C. L. Hill, *Inorg. Chem.*, 2007, 46, 5398; Q. Wu, Y.-G. Li, Y.-H. Wang, E.-B. Wang, Z.-M. Zhang and R. Clérac, *Inorg. Chem.*, 2009, 48, 1606; I. M. Mbomekalle, B. Keita, M. Nierlich, U. Kortz, P. Berthet and L. Nadjo, *Inorg. Chem.*, 2003, 42, 5143.
- 9 B. Godin, J. Vaissermann, P. Herson, L. Ruhlmann, M. Verdauger and P. Gouzerh, *Chem. Commun.*, 2005, 5624.
- 10 Z. Zhang, S. Yao, Y. Qi, Y. Li, Y. Wang and E. Wang, *Dalton Trans.*, 2008, 3051.
- 11 S. S. Mal and U. Kortz, *Angew. Chem., Int. Ed.*, 2005, 44, 3777; S. S. Mal, M. H. Dickman, U. Kortz, A. M. Todea, A. Merca, H. Bögge, T. Glaser, A. Müller, S. Nellutla, N. Kaur, J. van Tol, N. S. Dalal, B. Keita and L. Nadjo, *Chem.-Eur. J.*, 2008, 14, 1186; S. G. Mitchell, D. Gabb, C. Ritchie, N. Hazel, D.-L. Long and L. Cronin, *CrystEngComm*, 2009, 11, 36.
- 12 C. Ritchie, A. Ferguson, H. Nojiri, H. N. Miras, Y.-F. Song, D.-L. Long, E. Burkholder, M. Murrie, P. Kögerler, E. K. Brechin and L. Cronin, *Angew. Chem., Int. Ed.*, 2008, 47, 5609; Z. Luo, P. Kögerler, R. Cao and C. L. Hill, *Inorg. Chem.*, 2009, 48, 7812; P. Mialane, A. Dolbeq, E. Rivière, Jérôme Marrot and F. Sécheresse, *Angew. Chem., Int. Ed.*, 2004, 43, 2274.
- 13 X. Zhang, K. Sasaki and C. L. Hill, *J. Am. Chem. Soc.*, 1996, 118, 4809; Y. V. Geletii, B. Botar, P. Kögerler, D. A. Hillesheim, D. G. Musaev and C. L. Hill, *Angew. Chem., Int. Ed.*, 2008, 47, 3896.
- 14 S. P. Harmalkar, M. A. Lejarulo and M. T. Pope, *J. Am. Chem. Soc.*, 1983, 105, 4286; M. Abbessi, R. Contant, R. Thouvenot and G. Hervé, *Inorg. Chem.*, 1991, 30, 1695; R. Contant, M. Abbessi, J. Canny, A. Belhouari, B. Keita and L. Nadjo, *Inorg. Chem.*, 1997, 36, 4961.
- 15 T. M. Anderson, K. I. Hardcastle, N. Okun and C. L. Hill, *Inorg. Chem.*, 2001, 40, 6418.
- 16 T. L. Jorris, M. Kozik, N. Casañ-Pastor, P. J. Dommelle, R. G. Finke, W. K. Miller and L. C. W. Baker, *J. Am. Chem. Soc.*, 1987, 109, 7402.
- 17 Z. Zhang, Y. Li, Y. Wang and E. Wang, *Inorg. Chem.*, 2008, 47, 7615; B. Godin, Y.-G. Chen, J. Vaissermann, L. Ruhlmann, M. Verdauger and P. Gouzerh, *Angew. Chem., Int. Ed.*, 2005, 44, 3072; D. A. Judd, Q. Chen, C. F. Campana and C. L. Hill, *J. Am. Chem. Soc.*, 1997, 119, 5461.
- 18 A. P. Ginsberg, *Inorganic Synthesis*, 1990, 27, 108–109.
- 19 S. G. Mitchell, S. Khanra, H. N. Miras, T. Boyd, D.-L. Long and L. Cronin, *Chem. Commun.*, 2009, 2712.
- 20 Y.-W. Li, Y.-G. Li, Y.-H. Wang, X.-J. Feng, Y. Lu and E.-B. Wang, *Inorg. Chem.*, 2009, 48, 6452.
- 21 I.-M. Mbomekalle, Y. W. Lu, B. Keita and L. Nadjo, *Inorg. Chem. Commun.*, 2004, 7, 86; C. R. Graham and R. G. Finke, *Inorg. Chem.*, 2008, 47, 3679.
- 22 G. M. Sheldrick, *Acta Crystallogr., Sect. A: Found. Crystallogr.*, 1990, 46, 467.
- 23 G. M. Sheldrick, *Acta Crystallogr., Sect. A: Found. Crystallogr.*, 2008, 64, 112.
- 24 L. J. Farrugia, *J. Appl. Crystallogr.*, 1999, 32, 837.
- 25 R. C. Clark and J. S. Reid, *Acta Crystallogr., Sect. A: Found. Crystallogr.*, 1995, 51, 887.
- 26 The presence of other transition metals is known to suppress the tungsten signal for similar polyoxometalate clusters, whilst the observed value is within the $\pm 5\%$ error limit: S. G. Mitchell, C. Ritchie, D.-L. Long and L. Cronin, *Dalton Trans.*, 2008, 1415.
- 27 S. J. Dong, X. D. Xim and M. Tian, *J. Electroanal. Chem.*, 1995, 385; B. Keita and L. Nadjo, *J. Electroanal. Chem. Interfacial Electrochem.*, 1987, 227, 77; B. Keita, A. Belhouari, L. Nadjo and R. Contant, *J. Electroanal. Chem. Interfacial Electrochem.*, 1988, 247, 157; I.-M. Mbomekalle, B. Keita, Y. W. Lu, L. Nadjo, R. Contant, N. Belai and M. T. Pope, *Eur. J. Inorg. Chem.*, 2004, 276.
- 28 A. Belhouari, B. Keita, L. Nadjo and R. Contant, *New J. Chem.*, 1998, 22, 83.
- 29 B. S. Bassil, U. Kortz, A. S. Tigan, J. M. Clemente-Juan, B. Keita, P. de Oliveira and L. Nadjo, *Inorg. Chem.*, 2005, 44, 9360.